Supporting Information

Introduction of Sidewall C≡N: High-temperature-resistant COF for Lithium-ion Storage

Jiahui Yuan,[a] Zhenyu Zhang,[b] Yajie Feng,[c] Fuzhou Chen,[a] Wei Ding,[d] Yizi Zhang,[a] Hongxing Jia,[b] Zhengrong Gu[a]**

[a.] Department of Agricultural and Biosystems Engineering, South Dakota State University, Brookings, SD, 57007, USA.

[b.] College of Materials Science and Engineering, National Engineering Research Center for Magnesium Alloys, Chongqing University, Chongqing 400044, China.

[c.] College of Physics and Center of Quantum Materials and Devices, Chongqing University, Chongqing 401331, China.

[d.] Department of Electrical Engineering and Computer Science, South Dakota State University, Brookings, SD 57007, USA.

1. Material characterization

The morphology of the samples was characterized using Scanning Electron Microscopy (SEM, Thermo Fisher Scientific Quattro S) and Transmission Electron Microscopy (TEM, Thermo Fisher Scientific Talos F200S), with High-Angle Annular Dark Field Scanning Transmission Electron Microscopy (HAADF-STEM) images and corresponding Energy Dispersive X-ray Spectroscopy (EDS) mapping acquired using a FEI Titan Themis. X-ray diffraction (XRD) patterns were recorded using a PANalytical X'Pert Powder diffractometer equipped with Cu-Kα radiation (40 kV, 40 mA), at a scan rate of 5° min^{-1} and a 2θ angle range from 5° to 90°. Surface composition was analyzed using X-ray Photoelectron Spectroscopy (XPS) on a Thermo Fisher Scientific ESCALAB 250Xi, with all spectra calibrated to a C1s peak at 284.8 eV. Nitrogen adsorption-desorption isotherms were measured using Micromeritics analyzer (ASAP2460) to calculate the specific surface area and pore size distribution. Fourier-transform infrared (FT-IR) spectroscopy measurements were conducted using Thermo Fisher Scientific instrument (Nicolet iS10). Raman spectra were collected using HORIBA Jobin Yvon S.A.S. Raman spectrometer (LabRAM HR Evolution).

2. Electrochemical measurements

The electrochemical performances of the samples are evaluated in CR2032-type coin cells. The working electrodes were made up of active material, conducting carbon and polyvinylidene fluoride (PVDF) binder (the ratio of 8:1:1), formed with NMP solvent, coated on copper foil. The as-prepared working electrodes were dried in a vacuum oven at 80℃ for 12 h. The average loading mass of these active materials was about 0.8 mg cm^{-2}. In Li-ion batteries (LIBs), lithium foil acts as counter electrode and reference electrode, Celgard 2320 acts as separator, and 1 M $LiPF_6$ in ethylene carbonate (EC)/dimethyl carbonate (DMC)/ethyl methyl carbonate (EMC) (1:1:1 wt %)

with 5% fluoroethylene carbonate (FEC) acts as electrolyte. The cycling and rate performance was tested on a LANHE battery test system (CT3002A, Wuhan Land Electronics Co., Ltd.) with a voltage ranging from 0.01-3.0 V. The cyclic voltammetry (CV) curves were recorded within a voltage window of 0.01–3.0 V at various scan rates using an electrochemical workstation (CHI-760E, Shanghai Chen Hua Instrument Co., Ltd.). The electrochemical impedance spectroscopy (EIS) was performed at a frequency ranging from 0.01 Hz to 100 kHz using CHI-760E electrochemical workstation. All measurements were conducted at room temperature.

3. Lithium-Ion Diffusion Analysis by EIS

To calculate the lithium-ion diffusion coefficient using EIS, the following equation (1) was applied[1].

$$D = 0.5\left(\frac{RT}{n^2F^2ACA_w}\right)^2 \quad (1)$$

where D is the lithium-ion diffusion coefficient, R is the gas constant, T is the absolute temperature, n is the number of reacting electrons, F is the Faraday's constant, A is the area of the cathode/electrolyte interface (1.54 cm^2 in this work), C is the concentration of lithium-ion, and A_w is the Warburg factor which has relationship with Z′:

$$Z' = R_s + R_{ct} + A_w\omega^{-\frac{1}{2}} \quad (2)$$

where ω is the angular frequency ($\omega=2\pi f$).

The calculated lithium-ion diffusion coefficients for NPC_{700}, NPC_{800}, and NPC_{900} before cycling are 2.5×10^{-13} cm^2 s^{-1}, 4.1×10^{-13} cm^2 s^{-1} and 1.9×10^{-13} cm^2 s^{-1}, respectively. After cycling, the lithium-ion diffusion coefficients for NPC_{700}, NPC_{800}, and NPC_{900} are 5.2×10^{-13} cm^2 s^{-1}, 2.5×10^{-13} cm^2 s^{-1} and 6.5×10^{-13} cm^2 s^{-1}, respectively. NPC_{900} demonstrates a significantly higher lithium-ion

diffusion coefficient than NPC_{700} and NPC_{800} after cycling. Additionally, Fig. S8 and S9 illustrate the relationship between Z' and $\omega^{-1/2}$ at low frequency regions of NPC_{700}, NPC_{800}, and NPC_{900}.

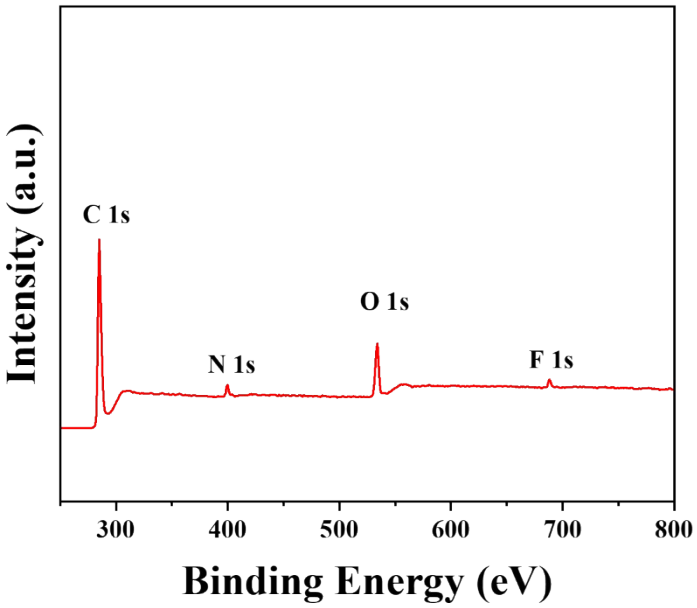

Figure S1. XPS survey spectra of COF-HHTP-CN.

Table. S1. The surface area retention of NPC_{700} and other N-rich COFs derived NPC materials in literature.

Materials	Pyrolysis temperature /℃	Surface area before pyrolysis /m^2 g^{-1}	Surface area after pyrolysis /m^2 g^{-1}	Surface area retention	Ref.
NPC_{700}	**700**	**531.7**	**358.8**	**67.5%**	**This work**
NC-700	700	601.4	52.4	8.7%	[2]
graphenic carbon	370	1290	517	40.1%	[3]
N doped carbon	/	2067	150	7.3%	[4]
COF_{700}	700	1189	561	47.2%	[5]
Co-CM-5	600	1458	244	16.7%	[6]
$Co@COF_0$	700	2143.54	573.11	26.7%	[7]
$Co–C500_{COF}$	500	717.94	351.89	49.0%	[8]
NC-700	700	999	408	40.8%	[9]

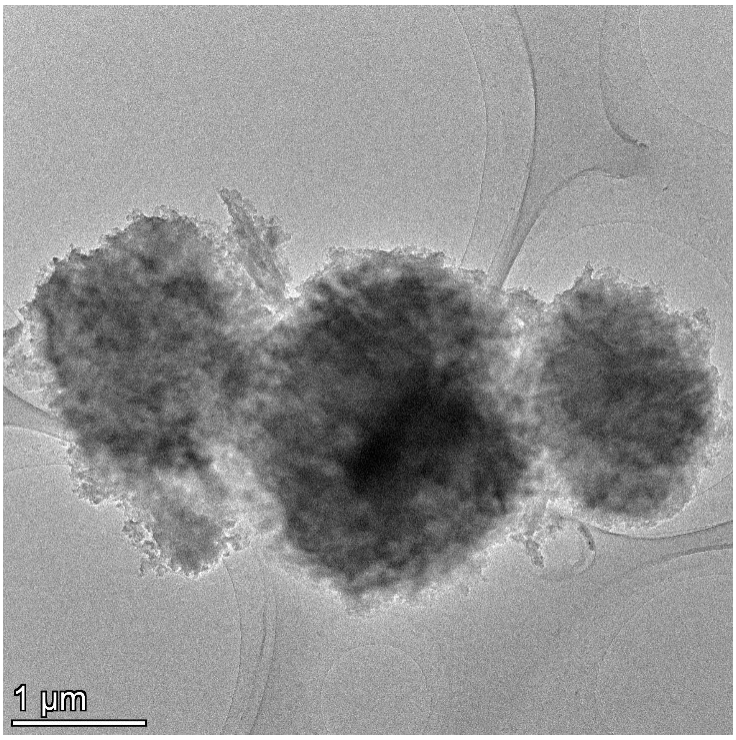

Figure S2. TEM image of COF-HHTP-CN.

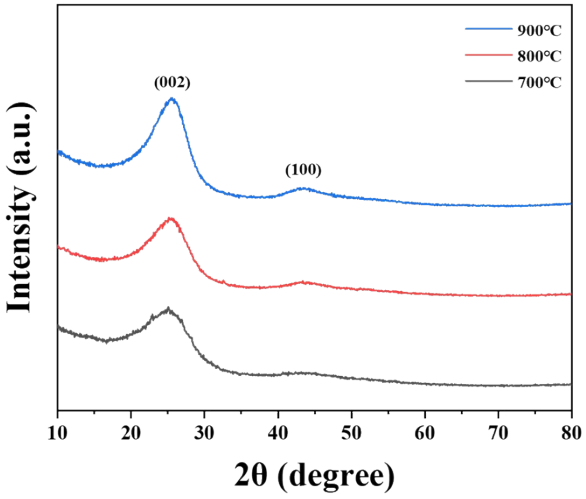

Figure S3. XRD spectra of NPC_{700}, NPC_{800}, and NPC_{900}.

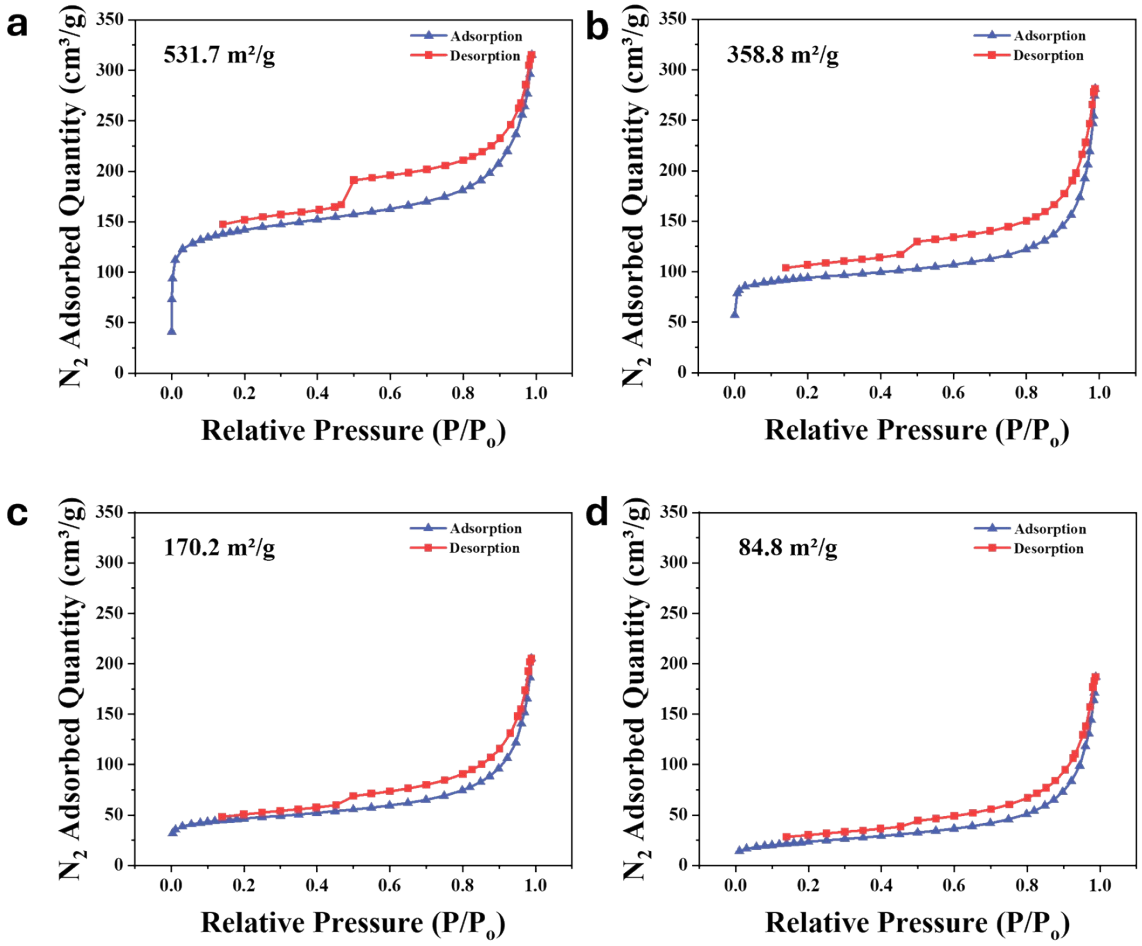

Figure S4. (a-d) N_2 adsorption/desorption isotherms of COF-HHTP-CN, NPC_{700}, NPC_{800} and NPC_{900}.

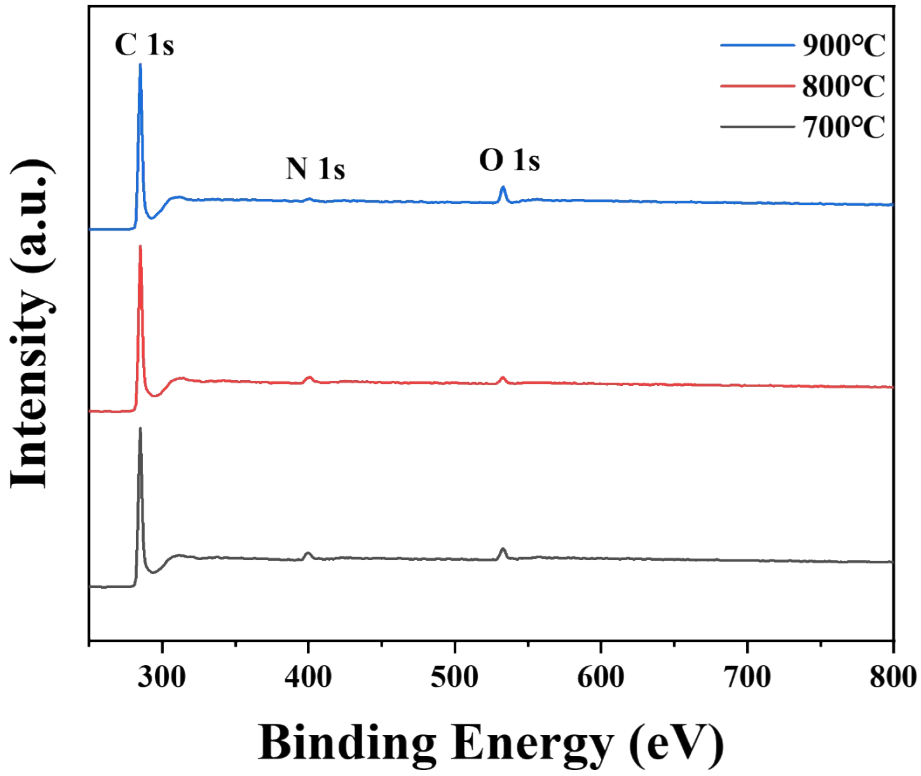

Figure S5. XPS survey of NPC_{700}, NPC_{800}, and NPC_{900}.

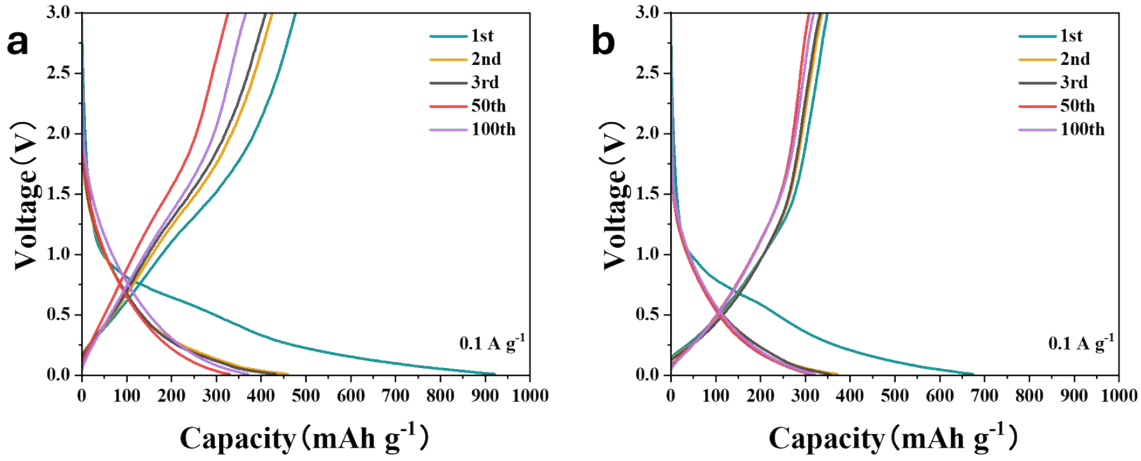

Figure S6. Galvanostatic charge-discharge tests of (a) NPC_{700} and (b) NPC_{900} at 0.1 A g^{-1}.

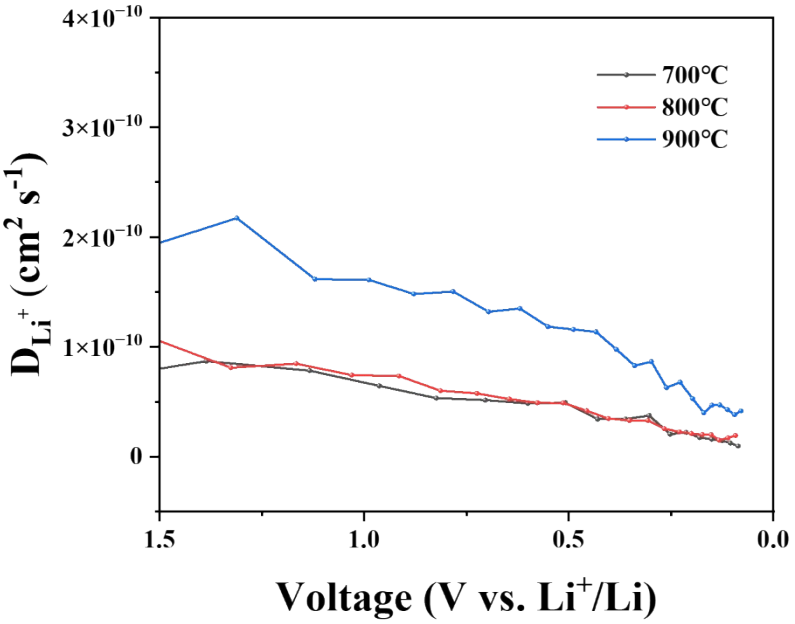

Figure S7. The lithium-ion diffusion coefficient of NPC_{700}, NPC_{800} and NPC_{900} in the discharging process.

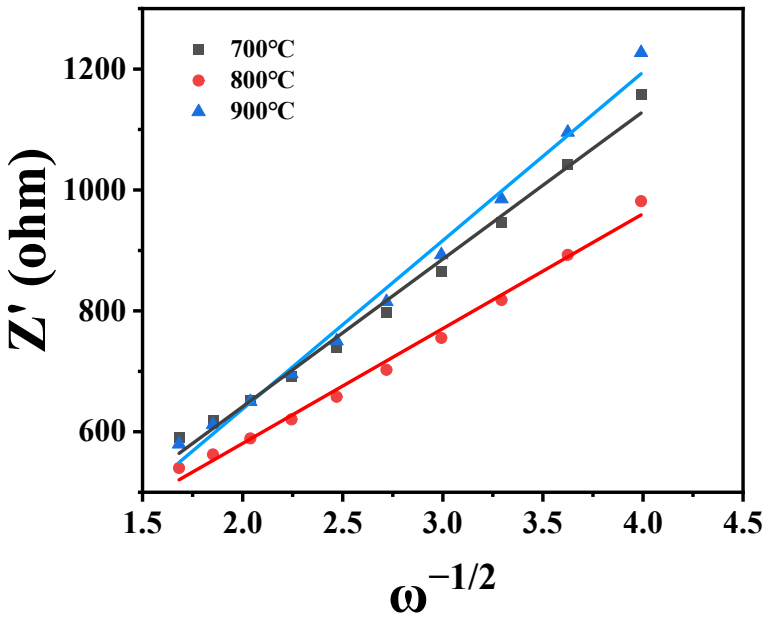

Figure S8. The relationship between Z' and $\omega^{-1/2}$ at low frequency regions of NPC_{700}, NPC_{800} and NPC_{900} before cycling. The calculated lithium-ion diffusion coefficients for NPC_{700}, NPC_{800}, and NPC_{900} before cycling are 2.5×10^{-13} cm^2 s^{-1}, 4.1×10^{-13} cm^2 s^{-1} and 1.9×10^{-13} cm^2 s^{-1}, respectively.

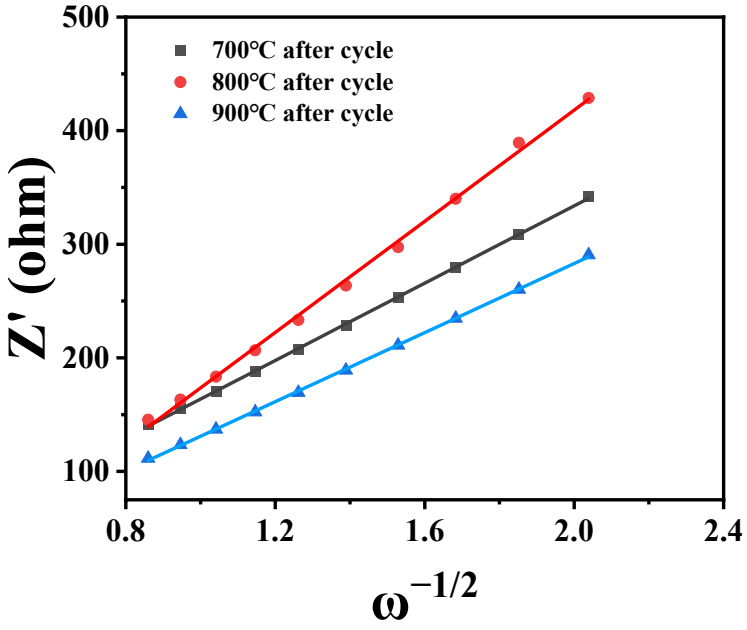

Figure S9. The relationship between Z' and $\omega^{-1/2}$ at low frequency regions of NPC_{700}, NPC_{800} and NPC_{900} after cycling. After cycling, the lithium-ion diffusion coefficient for NPC_{900} is calculated to be 6.5×10^{-13} cm^2 s^{-1}, surpassing those of NPC_{700} (5.2×10^{-13} cm^2 s^{-1}) and NPC_{800} (2.5×10^{-13} cm^2 s^{-1}).

References

1. L. Wang, J. Zhao, X. He, J. Gao, J. Li, C. Wan and C. Jiang, *Int. J. Electrochem. Sci.*, 2012, **7**, 345-353.
2. X. Hu, Y. Long, M. Fan, M. Yuan, H. Zhao, J. Ma and Z. Dong, *Appl. Catal., B*, 2019, **244**, 25-35.
3. D. Chakraborty, S. Nandi, R. Illathvalappil, D. Mullangi, R. Maity, S. K. Singh, S. Haldar, C. P. Vinod, S. Kurungot and R. Vaidhyanathan, *ACS Omega*, 2019, **4**, 13465-13473.
4. C. Yang, S. Maenosono, J. Duan and X. Zhang, *ChemNanoMat*, 2019, **5**, 957-963.
5. M. Liu, X. Zhu, Y. Song, G. Huang, J. Wei, X. Song, Q. Xiao, T. Zhao, W. Jiang, X. Li and W. Luo, *Adv. Funct. Mater.*, 2023, **33**, 2213395.
6. S. Liu, Y. Shuai, X. Qi, Z. Ding and Y. Liu, *Nano Res.*, 2024, **17**, 7068–7076.
7. M. Yao, M. Xie, S. Zhang, J. Yuan, L. Zhao and R.-S. Zhao, *Sep. Purif. Technol.*, 2022, **302**, 122145.
8. M. Cao, J. Lei, J. Zhang, L. Zhou and Y. Liu, *J. Cleaner Prod.*, 2022, **375**, 134114.
9. J. Lv, P. Hu, J. Zheng, S. Mo, W. Liu, S. Chen and Y. Liu, *J. Power Sources*, 2024, **602**, 234339.